



PAPER

Wafer-level fabrication of alkali vapor cells using in-situ atomic deposition

OPEN ACCESS

RECEIVED
7 August 2020REVISED
30 October 2020ACCEPTED FOR PUBLICATION
18 November 2020PUBLISHED
14 December 2020

Original Content from
this work may be used
under the terms of the
[Creative Commons
Attribution 4.0 licence](#).

Any further distribution
of this work must
maintain attribution to
the author(s) and the title
of the work, journal
citation and DOI.

D G Bopp^{1,2,3} , V M Maurice^{1,2} and J E Kitching²¹ Department of Physics, University of Colorado, Boulder, Boulder, CO 80302, United States of America² Time and Frequency Division, National Institute of Standards and Technology, Boulder, CO 80305, United States of AmericaE-mail: DougBopp@VaporCellTechnologies.com**Keywords:** microfabricated vapor cells, parallel fabrication, compact atomic devices, atomic spectroscopy**Abstract**

We demonstrate a new technique for filling mm-scale microfabricated silicon and glass cavities with alkali vapors at the wafer-scale. A single etched silicon wafer contains an array of cavities containing alkali precursor materials offset laterally from the cell array. The wafer is heated to create an array of alkali droplets on an upper glass wafer, which is then translated laterally under vacuum and bonded to create the cells. This technique can be implemented in a commercially available bonding tool, allows the fabrication of cells with arbitrary buffer gas contents and pressures and can potentially produce cells with dimensions below 100 μm .

1. Introduction

Alkali vapor cells are important building blocks for microwave and optical frequency references [1], as well as for precision magnetic [2, 3] and electric field [4] measurement instruments and other novel devices [5]. Fabricating these vapor cells is typically a complex and costly procedure because pure alkali metal, which is highly reactive with oxygen and water and readily consumed by glass at elevated temperatures, must be produced and distilled in an inert environment. Early demonstrations of microfabricated vapor cells used either direct deposition of alkali metal with a pipette [6] or in-situ [7] or ex-situ [8] chemical reactions. A review of approaches to the fabrication of alkali vapor cells using micromachining techniques can be found in [9].

The parallel fabrication of alkali vapor cells, in which an entire wafer of cells is fabricated using a single process sequence, has only been partially realized and existing methods have significant limitations. For example, alkali metal can be generated in a cell through UV-dissociation of RbN_3 deposited into a cell cavity before bonding [7, 10]. However, the relative abundance of Rb and N_2 is determined by the stoichiometry of the reaction, and only a few μg of Rb metal can be created in cells of volume 1 mm^3 , and N_2 must necessarily be present. This precludes the fabrication of cells without buffer gases, which are needed for optical or Rydberg spectroscopy. A second wafer-level process is based on the dissociation of $\text{Rb}_2\text{CrO}_4/\text{Zr}/\text{Al}$ in pill form which is thermally activated with a laser post-bonding [11, 12]. In this case N_2 is getterd by the Zr/Al, making it challenging to include this buffer gas in the cell. Recently, it has been reported that some N_2 can remain in the cell after activation [5]. This technique has been used successfully with a non-evaporable getter to produce a Rb vapor cell suitable for a high-performance, 2-photon optical clock [13]. In both cases, the post-activation is done cell by cell with a laser and residual chemical precursors remain in the cell, which can cause changes in the gas pressure over time [8] and obscure optical access. Often, a second cavity is needed separated by the vapor cell by thin channels to prevent the precursors or residual reactants from obscuring the windows of the cell cavity after activation.

In this letter, we demonstrate a novel method for fabricating alkali vapor cells in which the precursors are placed in an array of entirely separate filling chambers offset from the cell array by $\sim 1 \text{ mm}$. By heating the entire wafer under vacuum, Rb metal can be condensed into droplets on a glass surface placed over the cell

³ Present address: Vapor Cell Technologies, LLC, Boulder, CO, United States of America.

array. The glass can then be translated laterally before bonding to move the alkali material into the cell cavities while leaving activated reactant residue behind in the ‘deposition chambers’. The technique overcomes many limits imposed by alternative techniques. It allows for cells to be created with arbitrary buffer gases (or no gas at all); is compatible with whole wafers; potentially allows for very small cells with dimensions considerably below 1 mm; avoids reactant contamination; can incorporate isotopically enriched alkali metal; and uses a commercial anodic bonding tool, obviating the need for a custom vacuum system.

Historically, one of the first techniques used to microfabricate vapor cells employed a glass ampule situated above the cell to emit a beam of alkali metal into a cell cavity preform before bonding. The production of alkali metal was achieved using the substitution reaction $\text{BaN}_6 + 2\text{RbCl} \rightarrow \text{BaCl}_2 + 3\text{N}_2 + 2\text{Rb}$ [14] and enabled the separation of the reactants from the products. This proved important due to the observation of large drifts in vapor cells that retained both the reactants and products in the same chamber [8].

We adapt this technique to the wafer-scale by designing microstructures which incorporate the function of the alkali beam source into the wafer itself. This alleviates the complexity associated with having a retractable alkali beam source and permits arrayed fabrication using a single silicon wafer that contains both deposition cavities containing the reactants and the final cells themselves.

2. Experiment

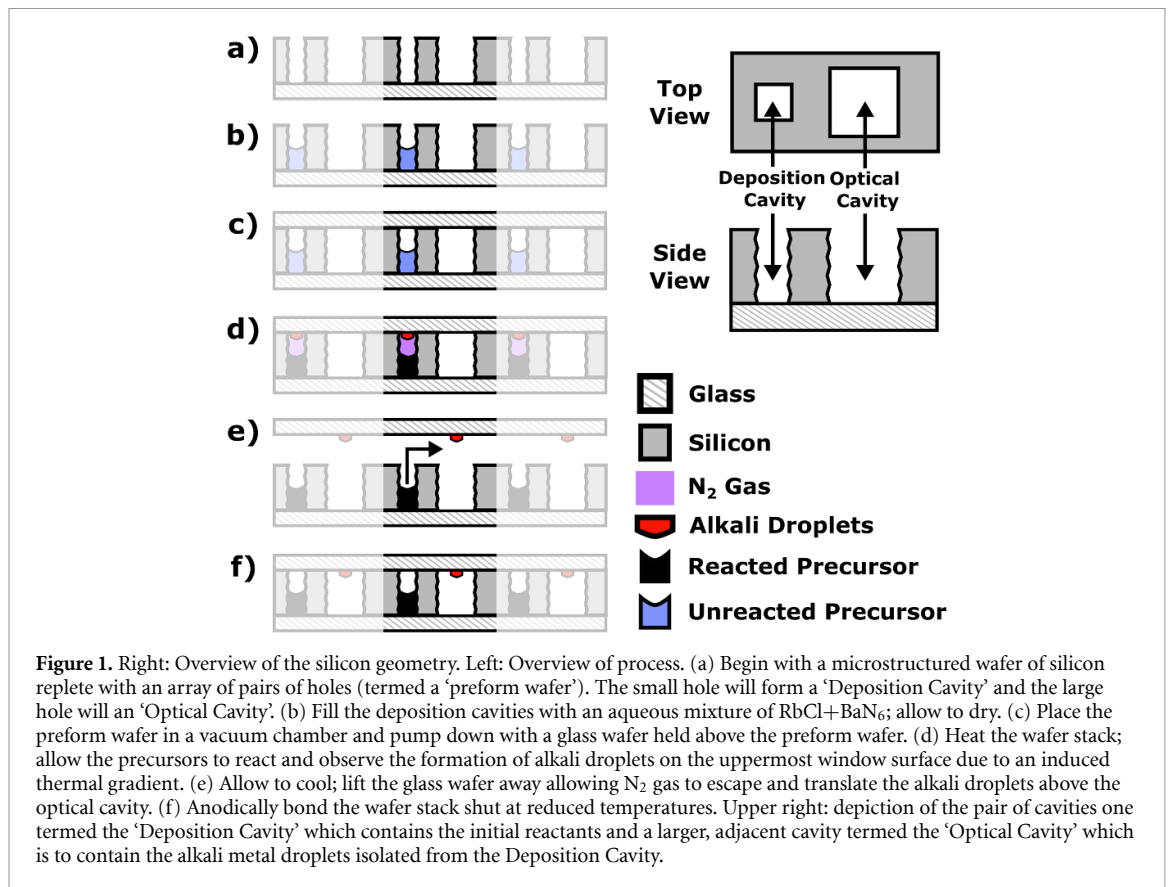
We start with a silicon wafer 1 mm thick and 4 inches in diameter polished on both sides. In this wafer, we etch two arrays of holes using deep reactive ion etching, spaced by pitch 6 mm, and offset laterally from each other by 3 mm (see figure 1(a)). The holes on one array, which we term the ‘deposition cavities’, are square with dimension 0.75 mm and are designed to hold the chemical precursors. The holes in the second array, which we term the ‘optical cavities’, are also square but with dimension 1 mm, and will ultimately form the final cells. The ‘unit cell’ of this wafer is therefore composed of two cavities.

The silicon wafer is bonded to a standard borosilicate wafer (500 μm thickness) resulting in a ‘preform wafer’ with open holes on one side. The deposition cavities of this preform wafer are then filled with an aqueous solution of $\text{BaN}_6 + \text{RbCl}$ using an automated pipetting system. The wafer is heated to 85 °C for 1 h to evaporate the water and leave a dried residue. This filled preform wafer is then inserted into an anodic bonding machine along with a second, standard borosilicate wafer (500 μm thickness) and placed under vacuum. The anodic bonding machine (AML AWB-04; Disclaimer: Certain commercial equipment is identified in this paper to foster understanding. Such identification does not imply recommendation or endorsement by the National Institute of Standards and Technology, nor does it imply that the materials or equipment identified are the best available for the purpose) is designed to allow the wafers to be moved with respect to one another under vacuum for alignment purposes. The two wafers are then brought into contact and the lower wafer is heated causing the precursors to react and evolve Rb and N_2 gas. Due to the thermal gradient from the asymmetric heating profile, Rb droplets condense onto the lower surface of the upper glass wafer. The wafers are then passively cooled (typically overnight), decreasing the vapor pressure of the Rb and then pulled apart, releasing the N_2 gas and allowing a second gas to be introduced if desired. The glass wafer with Rb droplets is then translated laterally and the droplets are positioned over the optical cavity. The two wafers are pushed together into contact and now the upper wafer is heated to 200 °C to enable a low-temperature anodic bond that takes place over 5 h. The thermal gradient is reversed and the Rb droplets are driven to the relatively cold preform wafer where they are not in contact with the hot glass surface to be bonded. A complete overview of this process is depicted in figure 1 on the left.

Two wafers were fabricated, one intended to contain evacuated cells with no residual gas, and the other where buffer gas is intentionally introduced at a known pressure into the chamber before the final anodic bonding step. After fabrication, optical spectroscopy on each cell on both wafers was performed at an elevated temperature with a laser, which we scanned across the Rb D_2 line. The temperature of the buffer-absent cells was of 67 °C and the temperature of the buffer-present cells was increased to of 90 °C due to the decreased absorbance. From these measurements an estimate of the broadening and shift of the optical resonances with respect to a reference evacuated Rb cell can be extracted and hence establish the amount of residual gas density in each cell on the wafer.

For the evacuated cells, 125 deposition cavities were filled with chemical precursors and 35 of the final cells demonstrated clear Rb absorption signatures for a yield of 28%. Figure 2(a) depicts the normalized logarithm of the absorption for all microfabricated cells compared to a standard reference cell (indicated in green). We assume the dominant residual gas is N_2 and use standard pressure broadening coefficients [15] to estimate the residual buffer gas pressure in each cell. A histogram of these pressures is shown in figure 2(b).

Most cells show some residual gas. This can be partially attributed to the method of cleaning the wafers after filling with the aqueous solution. As the solution dries, it may precipitate proud of the surface of the



preform wafer and prevent clean anodic bonding. This precipitate was cleaned but flakes were distributed into some of the optical cavities. While N_2 drying was applied to flush the flakes out of the preform, some flakes were likely left behind. These flakes are able to evolve N_2 when heated and may describe the variation in residual pressures in some of the cells see in figure 2.

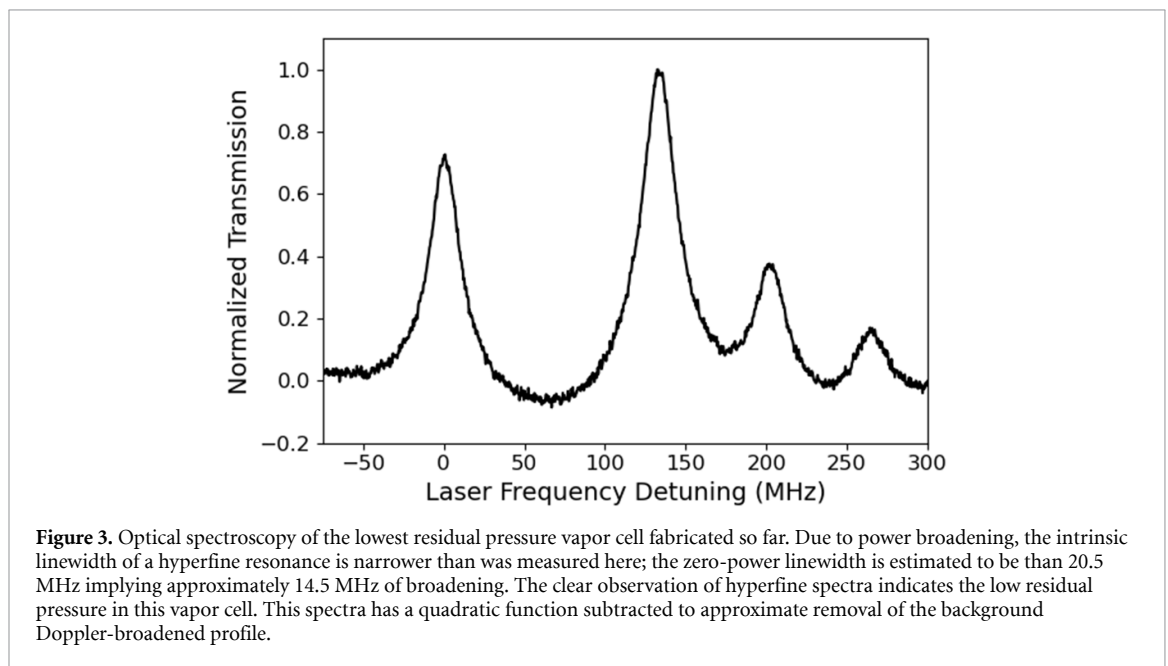
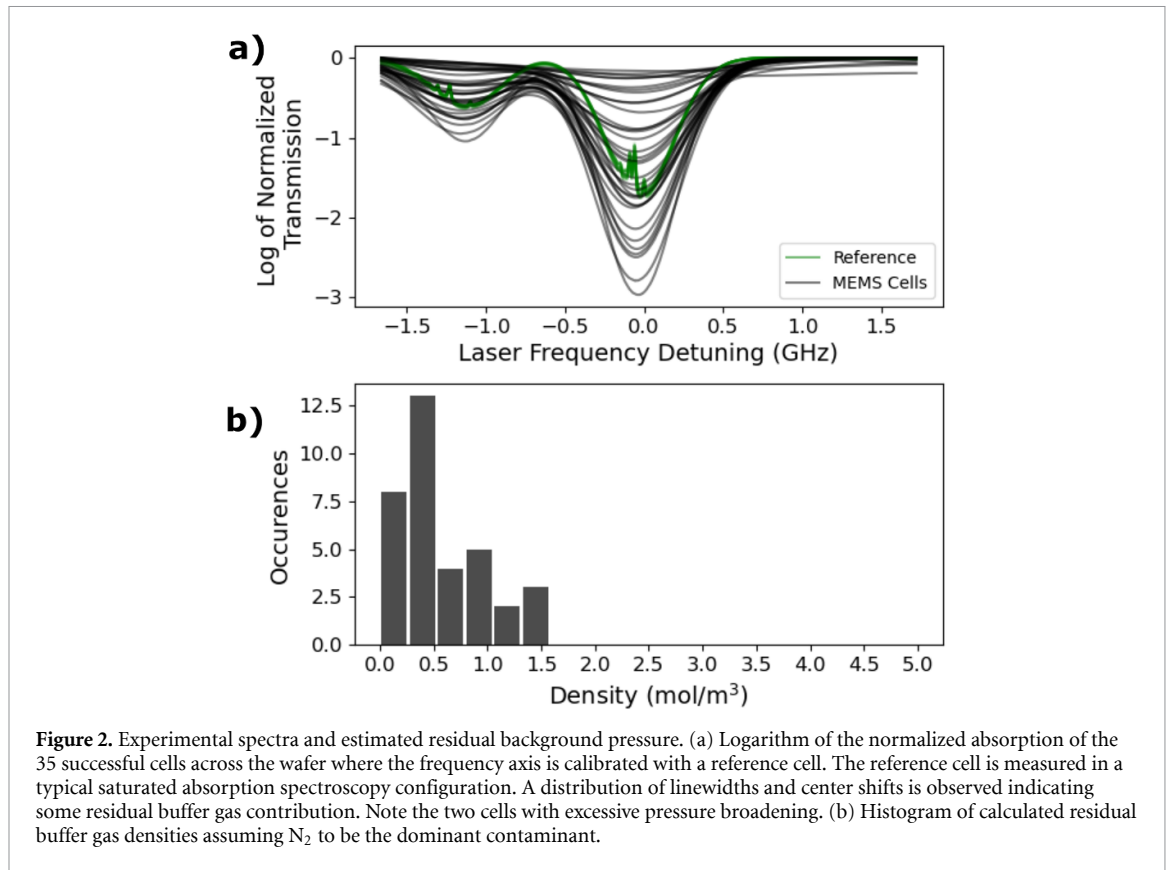
The cell with the lowest residual pressure was measured using saturated absorption spectroscopy (SAS) as a fine measure of residual gas content. One trace of this spectroscopy is depicted in figure 3. The linewidth was measured as a function of optical power to extract the zero-power linewidth, which was measured to be 20.5 MHz and includes broadening due to residual gases, the magnetic field gradient from the heater, the DBR linewidth (≈ 1 MHz), Rb-Rb collisions (< 100 kHz at an operating temperature of 67°C), and angular mismatch of the pump/probe beams (≈ 650 kHz). Subtracting the known confounding variables yields 14.5 MHz of broadening due to the combination of the magnetic field gradient and the residual pressure. Neglecting the magnetic field gradient, the estimated residual pressure is ≈ 0.1 kPa of N_2 gas at room temperature. The shift of the absorption spectrum was measured with respect to that of a reference cell to be less than 2.5 MHz implying a residual pressure of ≈ 0.06 kPa.

The optical density also shows a distribution due to the impact of the buffer gas collisions on the atomic absorption cross section. However, due to variable beam clipping and the variable impact of optical pumping in each cell depending on the pressure, the extraction of the buffer gas pressure using optical density measurements contains greater uncertainty than the prior analysis.

This best cell indicates that sub-kPa residual pressures are achievable and further process refinements can reduce the distribution of residual pressures in these cells.

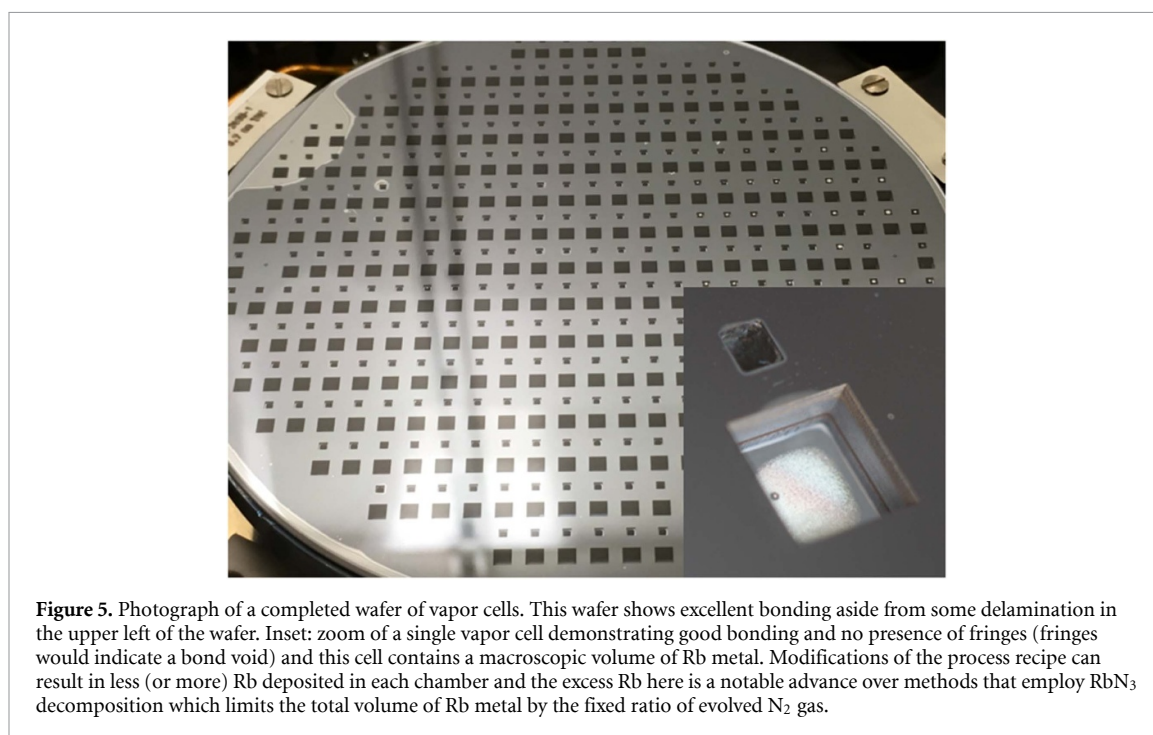
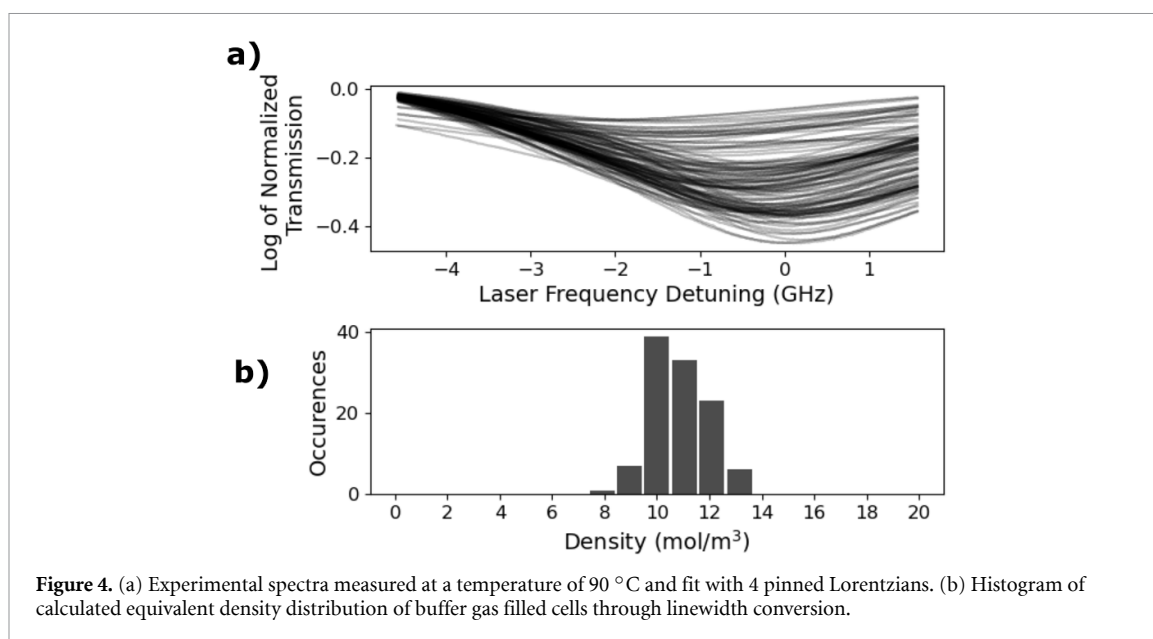
The intentional addition of a buffer gas at the few tens of kPa level reduces wall relaxation, enables efficient optical pumping and reduces Doppler broadening of microwave transitions of atoms in the cell. A buffer gas is therefore a desirable feature of CPT atomic clocks and magnetometers.

A wafer of buffer gas cells was fabricated as follows. After the Rb droplets are deposited on the upper glass wafer surface and the wafer stack is allowed to cool (step d in figure 1), the wafers are lifted apart and any residual N_2 gas evolved during the reaction is pumped away. After cooling to room temperature, the bonding chamber is backfilled with N_2 at a pressure of 28 ± 1 kPa at a temperature of approximately 35°C , measured after a gate valve connecting the chamber to the vacuum pumps is closed. This corresponds to approximately 11.2 mol m^{-3} (0.25 amg) of N_2 gas within the chamber. The wafers are pressed together and then bonded at



a temperature of 200 °C. In this case, the wafer was patterned with 499 cavity pairs, of which 350 were filled with precursors. After bonding, Rb absorption was observed in 109 optical cavities for a yield of 31%.

The optical spectra of the cells in the second wafer are shown in 4(a). We simplify the hyperfine structure by approximating the manifold as a single resonance positioned in the center of mass of the hyperfine spectrum. The logarithm of the normalized transmission spectrum is taken and the resulting lineshape is fit to a sum of four Lorentzians with fixed relative amplitudes and center separations but variable linewidths corresponding to the ⁸⁵Rb F_g = 1 → F_e' = (0,1,2), ⁸⁵Rb F_g = 2 → F_e = (1,2,3), ⁸⁷Rb F_g = 2 → F_e = (1,2,3), and ⁸⁷Rb F_g = 3 → F_e = (2,3,4) resonances present in the D₂ absorption spectrum. Because the buffer gas linewidth broadening is an order of magnitude greater than the Doppler-broadening, we neglect the Doppler



broadening. The resulting Lorentzian linewidths are then used as a measure of the optical broadening due to the applied buffer gas density [16] and these linewidths are divided by $19.2 \text{ GHz amg}^{-1}$ to convert the homogeneous broadening into a buffer gas density estimate. The results of this fit are displayed in figure 4.

The results of this analysis result in a distribution of buffer gas pressures with a mean of 10.8 mol m^{-3} with a 1σ standard deviation of 1.1 mol m^{-3} . The mean estimated density in these vapor cells $10.8 \pm 1.1 \text{ mol m}^{-3}$ is consistent with the estimated density added $11.0 \pm 1.1 \text{ mol m}^{-3}$). A photograph of a completed wafer is shown in figure 5 with a typical cell shown inset. This photograph shows the ability to produce macroscopic quantities of alkali metal with a hermetic anodic bond with high uniformity.

3. Discussion

The process described here has several important advantages compared to existing methods of fabricating alkali vapor cells. First, it is a wafer-level process allowing many cells to be fabricated with a single process sequence. It uses commercially available bonding equipment, removing the need for designing a custom vacuum apparatus. Since the reactants other than the alkali metal remain in the deposition chambers, the

cells contain few impurities which can cause long-term drifts in the buffer gas pressure and corresponding frequency drifts in atomic clocks [8]. Furthermore, the ability to decouple the volume of alkali metal produced from the final buffer gas pressure allow for arbitrary quantities of alkali metal to be contained in the cells as well as arbitrary buffer gas compositions and pressures limited only by buffer gases that would impede anodic bonding. By using microfabricated alkali effusion cells to deposit the alkali metal into the optical cavity, we achieve higher spatial localization of the metal than typically achieved through usual micropipetting. As a result, it may be possible to fabricate alkali vapor cells with dimensions well below 1 mm, and possibly as small as 50 μm . Such cells would further enable the integration of photonic devices with atomic vapors [17]. Small dimension cells also offer reductions in operational power and may enable new applications heretofore not realized.

4. Conclusion

In summary, we demonstrate a novel technique to produce alkali vapor cells at the wafer-scale using microfabricated alkali effusion cells integrated directly into the same wafer that forms the alkali optical cavities. We demonstrate clean, macroscopic quantities of rubidium with no residual precursor in the optical cavity in an anodically bonded package. We also demonstrate the mass fabrication of buffer gas alkali vapor cells with a narrow distribution of buffer gas pressures suitable for optical magnetometers. The capability to backfill with arbitrary buffer gas pressures and species overcomes the limitations of alternative wafer-level alkali vapor cell fabrication techniques.

Author's contributions

DGB and VMM contributed equally to this work.

Data availability

The data that support the findings of this study are available from the corresponding author upon reasonable request.

Acknowledgments

This work was performed at the National Institute of Standards and Technology using internal funding. Thanks to Jennifer Black and Matthew Simmons for helpful comments on the manuscript. Thanks to Susan Schima for processing expertise and time.

ORCID iD

D G Bopp  <https://orcid.org/0000-0002-9085-766X>

References

- [1] Arditi M and Carver T R 1958 Optical detection of zero-field hyperfine splitting of Na23 *Phys. Rev. Lett.* **109** 1012–13
- [2] Dehmelt H G 1957 Modulation of a light beam by precessing absorbing atoms *Phys. Rev.* **105** 1924–5
- [3] Bell W E and Bloom A L 1957 Optical detection of magnetic resonance in alkali metal vapor *Phys. Rev.* **107** 1559–65
- [4] Sedlacek J A, Schwettmann A, Kübler H, Löw R, Pfau T and Shaffer J P 2012 Microwave electrometry with Rydberg atoms in a vapour cell using bright atomic resonances *Nat. Phys.* **8** 819–24
- [5] Noor R M, Asadian M H and Shkel A M 2020 Design Considerations for micro-glassblown atomic vapor cells *J. Microelectromech. Syst.* **29** 25–35
- [6] Liew Li A, Knappe S, Moreland J, Robinson H, Hollberg L and Kitching J 2004 Microfabricated alkali atom vapor cells *Appl. Phys. Lett.* **84** 2694–6
- [7] Liew Li A, Moreland J and Gerginov V 2007 Wafer-level filling of microfabricated atomic vapor cells based on thin-film deposition and photolysis of cesium azide *Appl. Phys. Lett.* **90** 132–4
- [8] Knappe S, Gerginov V, Schwindt P D D, Shah V, Robinson H G, Hollberg L and Kitching J 2005 Atomic vapor cells for chip-scale atomic clocks with improved long-term frequency stability *Opt. Lett.* **30** 2351
- [9] Kitching J 2018 Chip-scale atomic devices *Appl. Phys. Rev.* **5** 108–13
- [10] Karlen S, Gobet J, Overstolz T, Haesler J and Lecomte S 2017 Lifetime assessment of RbN₃-filled MEMS atomic vapor cells with Al₂O₃ coating *Opt. Express* **25** 525–31
- [11] Douahi A, Nieradko L, Beugnot J C, Dziuban J, Maillote H, Guerandel S, Moraja M, Gorecki C and Giordano V 2007 Vapour microcell for chip scale atomic frequency standard *Electron. Lett.* **43** 33–4
- [12] Hasegawa M, Chutani R K, Boudot R, Mauri L, Gorecki C, Liu X and Passilly N 2013 Effects of getters on hermetically sealed micromachined cesium–neon cells for atomic clocks *J. Micromech. Microeng.* **23** 055022
- [13] Newman Z L *et al* 2019 Architecture for the photonic integration of an optical atomic clock *Optica* **6** 680

- [14] Knappe S, Schwindt P D D, Gerginov V, Shah V, Liew L, Moreland J, Robinson H G, Hollberg L and Kitching J 2005 Microfabricated atomic clocks and magnetometers *IEEE/LEOS Optical MEMS 2005: Int. Conf. Optical MEMS and their Applications* vol 8 pp 193–4
- [15] Rotondaro M D and Perram G P 1997 Collisional broadening and shift of the rubidium D1 and D2 lines (52S12 to 52P12, 52P32) by rare gases, H₂, D₂, N₂, CH₄ and CF₄ *J. Quant. Spectrosc. Radiat. Transfer* **57** 497–507
- [16] Romalis M V, Miron E and Cates G D 1997 Pressure broadening of Rb D1 and D2 lines by 3 He, 4 He, N 2 and Xe: line cores and near wings *Phys. Rev. A* **56** 4569–78
- [17] Hummon M T *et al* 2018 Photonic chip for laser stabilization to an atomic vapor with 10–11 instability *Optica* **5** 443